The curious case of mobility reversal in sediment mixtures

THE CURIOUS CASE OF MOBILITY REVERSAL IN SEDIMENT MIXTURES

By Luca Solari[1] and Gary Parker[2]

ABSTRACT: It is common for aggrading deposits of sediment mixtures to show a pattern of downstream fining, whereby characteristic grain size becomes finer in the streamwise direction. Although various factors may contribute to this phenomenon, it can often be explained largely or solely in terms of the variation of grain mobility with grain size in sediment mixtures. That is, finer grains exposed on the surface are typically somewhat more mobile than their coarser neighbors, resulting in preferential transport of finer grains. Experiments reported here, document a reversal in this familiar pattern at slopes in excess of 0.02–0.03. At these higher slopes aggrading and prograding deposits are observed to show downstream coarsening in geometric mean size, indicating a mobility reversal associated with preferential transport of the coarser grains. This rather curious behavior is explored herein.

INTRODUCTION

It is common for rivers to exhibit downstream fining (i.e., a tendency for the characteristic size of the river bed material to become gradually finer in the downstream direction). The topic has attracted research interest for decades, as outlined in Shaw and Kellerhals (1982) and Sambrook Smith and Ferguson (1996). Several mechanisms have been postulated to explain this phenomenon, including abrasion (Shaw and Kellerhals 1982), selective transport of finer grains (Paola et al. 1992a,b), and a tendency for rivers to receive a successively finer sediment supply toward the downstream end of the basin (Pizzuto 1995). Depending upon the conditions of the stream and basin, it is likely that each of these mechanisms plays a role in establishing the pattern of fining.

Paola et al. (1992b), Seal et al. (1997), and Toro-Escobar et al. (unpublished paper 1999) reported on a set of six large-scale experiments (Runs 1–6) that demonstrated that downstream fining can be driven solely by selective transport of finer grains. In the experiments, here referred to as the DSF (downstream fining) experiments, a mix of durable sediments ranging in size from <0.1 to 90 mm was fed into a stream of water in a long flume and allowed to form an aggrading deposit that gradually prograded into standing water. The sediment was multimodal, with one sand and two gravel modes, and a minimum content in the neighborhood of 2 mm. Four of the runs (Runs 1–3 and 6) were performed in a channel with a width of 0.3 m; in the other two (Runs 4 and 5) the channel width was 2.7 m. All six experiments exhibited a gradual streamwise decline in both the D_{90} and D_{50} grain sizes (such that 90 and 50%, respectively, of a sample is finer) over a reach of 35–40 m. This pattern of fining was exhibited in both the surface and substrate sediment. In all cases except one, downstream fining was accompanied by a long profile that exhibited a mild upward concavity such that bed slope declined downstream. (In the case of the single exception, Run 4, a small number of pronounced alternate bars probably helped to obscure this concavity.) The fining pattern exhibited at the end of Run 5 (a wide run) is shown in Fig. 1.

Cui et al. (1996) showed that most features of the fining of gravel within the deposits of the narrow Runs 1–3 of the St. Anthony Falls Laboratory (SAFL) fining experiments could be explained using an existing formulation for the transport of poorly sorted gravel mixtures (Parker 1990) combined with an empirical transfer function for the deposition of gravel from bed load (Toro-Escobar et al. 1996). An extension of this formulation has been used to characterize the roles of both differential transport and abrasion on downstream fining at field scale (Parker 1991a,b; Cui and Parker 1998; Parker and Cui 1998).

The reader might think at this point that the nature of selective transport in driving downstream fining has been established beyond doubt. The idea that finer grains in a mixture are more mobile than coarser grains would, in addition, seem to be obvious. The problem is not so simple. A substantial amount of anecdotal evidence suggests that in the laboratory aggrading and prograding deposits formed from a poorly sorted sediment feed tend to exhibit downstream coarsening, not fining. For example, the second writer of this paper has observed a tendency for downstream coarsening in aggrading or prograding deposits in the laboratory under a variety of conditions, including flumes and radially expanding alluvial fans. The observed tendency is in direct contradiction with the contention that finer grains are more easily mobilized in a poorly sorted mix of sediment. This phenomenon is herein termed ''mobility reversal,'' according to which the coarse grains are more mobile than their finer siblings.

Anecdotal evidence notwithstanding, the phenomenon of downstream coarsening in aggrading or prograding laboratory deposits has only rarely been described in the literature. Two reasonably well-documented cases, however, are given by Straub (1935) and Kodama et al. (1992). The latter authors document an aggrading deposit with an upward concave profile. The feed sediment was bimodal, with sand and pea gravel modes and minimum content near 1 mm. Over a length of about 20 m, surface median grain size increased by a factor of 2 in the downstream direction as the bed slope declined by a factor of 2. Evidently the coarser grains in the sediment proved to have a higher mobility than their finer siblings. Kodama et al. characterized their result as follows (translating from Japanese): ''This observed fact completely contradicts common sense.''

The goal of this paper is a physically based explanation of this most curious and counterintuitive phenomenon of mobility reversal in sediment mixtures. The phenomenon is reproduced experimentally, and the resulting data are used to obtain that explanation.

HYPOTHESES FOR MOBILITY REVERSAL

In commencing the research, the writers considered three hypotheses for the observed mobility reversal:

[1]PhD Student, Dept. of Envir. Engrg., Univ. of Genova, Genova, Italy 16145.

[2]Prof., St. Anthony Falls Lab., Univ. of Minnesota, Mississippi River at 3rd Ave. SE, Minneapolis, MN 55414.

Note. Discussion open until August 1, 2000. To extend the closing date one month, a written request must be filed with the ASCE Manager of Journals. The manuscript for this paper was submitted for review and possible publication on November 10, 1998. This paper is part of the ***Journal of Hydraulic Engineering***, Vol. 126, No. 3, March, 2000. ©ASCE, ISSN 0733-9429/00/0003-0185–0197/$8.00 + $.50 per page. Paper No. 19615.

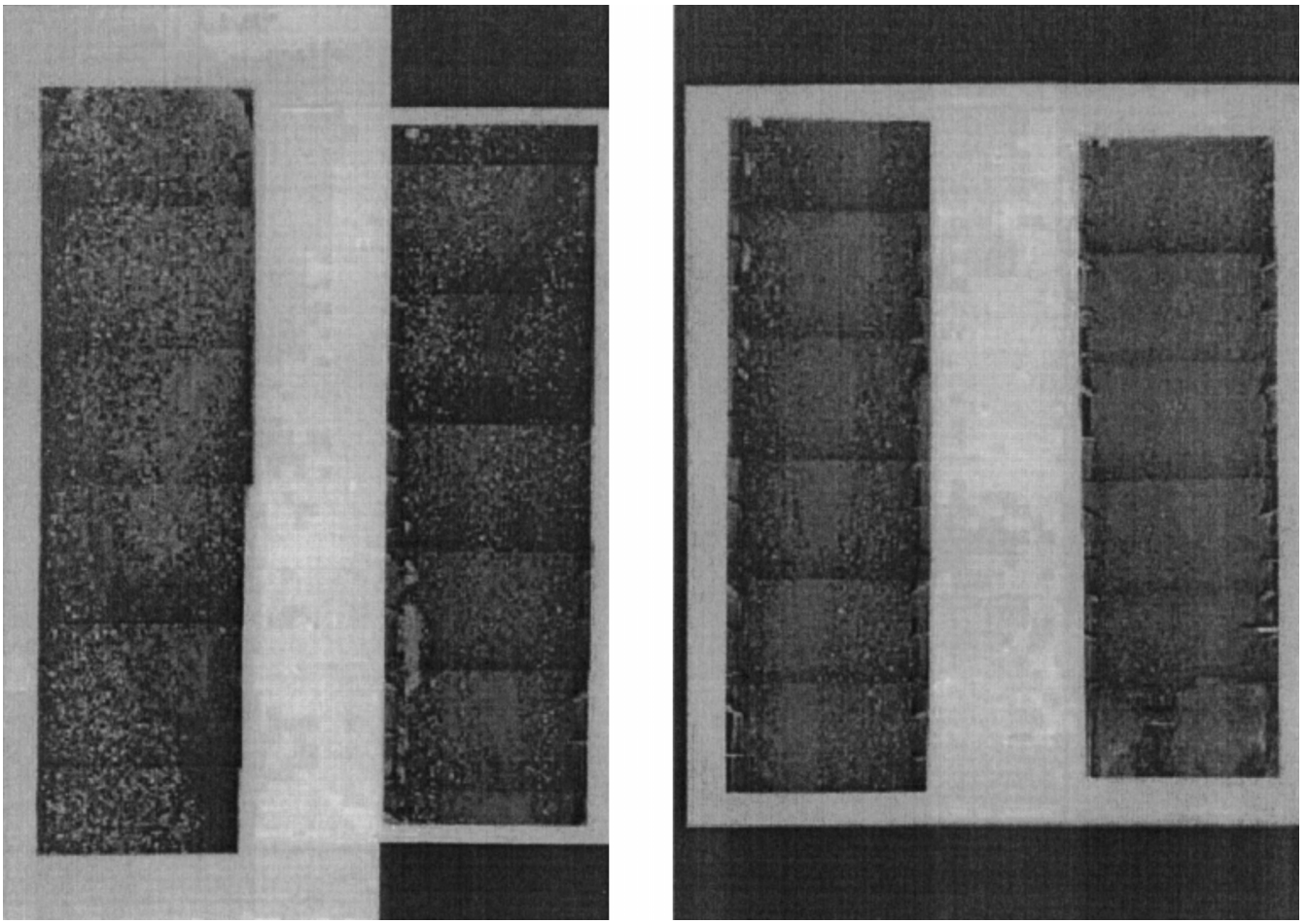

FIG. 1. View of Pattern of DSF Evident at the End of Run 5 of the DSF Experiments Performed at SAFL: (a) First 10 m from Feed Point; (b) Second 10 m; (c) Third 10 m; (d) Fourth and Final 10 m

- Viscous effects
- Flow blockage by the coarsest grains
- Sediment bimodality

Before introducing them, however, it is useful to review the standard reasoning according to which coarser grains are deemed to be less mobile than finer grains in a mixture.

Standard Model for Mobility Variation in Mixture

Assuming that all grains have the same specific gravity, coarser grains are heavier than finer grains, rendering them intrinsically less mobile. In a mixture, however, finer grains exposed at the surface tend to protrude less into the flow than coarser grains and therefore experience a reduced drag. The latter effect has been known as ''hiding'' since the time of Einstein (1950). Since the groundbreaking work of Egiazaroff (1965) and Ashida and Michiue (1972), it has been established that these two effects nearly cancel each other out [e.g., Wiberg and Smith (1987)] but nevertheless leave the finer grains exposed at the surface somewhat more mobile than neighboring coarser grains [e.g., Parker (1990)]. The residual difference in mobility tends to be small and, in particular, less than might be expected based on the scalings according to which particle weight increases with the cube of grain size whereas drag increases only with the square. This notwithstanding, it appears to be quite sufficient to drive downstream fining over reaches of sufficient length displaying upward concavity in the long profile (i.e., decreasing bed slope in the streamwise direction). One easy way to create such a long profile in the laboratory is to allow sediment deposition to create an aggradational or progradational long profile.

Hypothesis of Viscous Effects

Under this hypothesis it is assumed that the mobility reversal occurs only when the characteristic grain size of the sediment feed is sufficiently fine. In particular, it is assumed that the flow is not completely rough, so that a partial viscous sublayer may exist near the bed. The finer grains hide within the partial viscous sublayer, whereas the coarser grains protrude directly into the turbulence and are more easily entrained.

An appropriate scaling for viscous effects in the length scale δ_ν where

$$\delta_\nu = 11.6 \frac{\nu}{u_*} \tag{1}$$

where ν = kinematic viscosity of water; and u_* = shear velocity [e.g., Schlichting (1968)], here estimated using the simple assumption of normal (equilibrium) flow

$$u_* \cong \sqrt{gHS} \tag{2}$$

where H denotes flow depth; and S denotes streamwise bed slope. The controlling dimensionless ratio is assumed to be k_s/δ_ν, where k_s is an estimate of the roughness height of the bed. The parameter k_s can in turn be related to a characteristic size of the bed material exposed on the surface; that is

$$k_s = n_k D_{90} \tag{3a}$$

where n_k = order-one number typically between 1 and 4 and often taken to be close to 2. The ratio k_s/δ_ν is simply related to the Reynolds number R_k based on shear velocity and roughness height as

$$\frac{k_s}{\delta_v} = \frac{R_k}{11.6}; \quad R_k = \frac{u_* k_s}{\nu} \tag{3b,c}$$

Flow is typically considered to be hydraulically smooth for $R_k < 5$ or $k_s/\delta_v < 0.43$, and hydraulically rough for $R_k > 70$, or $k_s/\delta_v > 6.03$. For sufficiently coarse sediment k_s/δ_v thus becomes sufficiently large to preclude viscous effects. Gravel bed streams in the field tend to fall well into this range, within which a mobility reversal would not be expected. According to the hypothesis, a mobility reversal might occur when this ratio is not too far from unity. This in turn requires a sediment mix with a value of D_{90} that is not so large as to render viscous effects negligible.

With this in mind, consider a mobile bed with a mixture of sizes, such that k_s/δ_v is greater than unity but not too large (to allow for residual viscous effects) but such that, for example, $D_{10}/\delta_v < 1$. The implication is that the larger sizes feel the full effect of the turbulence but that the smaller sizes are protected by viscous effects, resulting in a mobility reversal. This hypothesis would appear to be supported because the coarsest grains in the experiments of Straub (1935) and Kodama et al. (1992) were only in the range of pea gravel.

Hypothesis of Flow Blockage

According to this hypothesis the mobility reversal occurs only when the flow is sufficiently shallow. The controlling dimensionless ratio is taken to be H/D_{90}. When this ratio becomes sufficiently small the coarser grains in the mix protrude sufficiently into the flow to interact with the water surface, creating a blocking effect that might amplify drag. The result would be an enhancement of the mobility of coarser grains at the expense of the finer grains. The hypothesis would appear to be supported by the shallowness of the flows in the experiments of Straub (1935) and Kodama et al. (1992).

Hypothesis of Bimodality

According to this hypothesis, in the case of strong bimodality the coarse grains can roll or slide smoothly over a bed of much finer grains, with few intermediate sizes to hinder motion. The governing dimensionless parameter is then $D_{\text{coarse}\,m}/D_{\text{fine}\,m}$, where $D_{\text{coarse}\,m}$ denotes the characteristic size of the coarse mode and $D_{\text{fine}\,m}$ denotes the characteristic size of the fine mode. The implication is that this parameter must be sufficiently large for mobility reversal. The bimodality of the experiments of Kodama et al. (1992) would appear to support this hypothesis. In the SAFL fining experiments, which were also bimodal (or rather trimodal, with one sand and two gravel modes), however, no mobility reversal was observed.

In the event, none of these hypotheses serves to explain the mobility reversal observed in the experiments discussed below. They did, however, offer a conceptual base from which to begin a quantitative investigation of the phenomenon.

EXPERIMENTAL SETUP AND PROCEDURE

The experimental setup was based on the principles of geometric and Froude scale modeling. Experiments were conducted in two flumes of differing size, such that the characteristic length scale of the experiments in the ''small'' flume was one third that of the ''large'' flume. The small flume had a width B of 0.05 m, a length of 1.98 m, and a depth of 0.40 m; the large flume had a width B of 0.15 m, a length of 10 m, and a depth of 0.39 m. Here the parameter of relevance is the width, for which the scaling ratio λ is indeed 1/3. It should be noted that the width of the large flume is still only half of that used in the narrow DSF runs. The two flumes were used to capture any scale effects, should they occur, on sediment sorting due to, for example, viscosity.

The size distribution of the feed sediments used in the experiments was scaled as closely as possible using a scaling ratio λ of 1/3. The size distributions used in the small and large flumes are shown in Fig. 2, along with the size distribution used in Runs 1–4 of the DSF experiments. The geometric mean size of the feed sediment D_{fg} in the small flume was 1.7 mm in the small flume and 5.1 mm in the large flume. The geometric standard deviation σ_{fg} of the feed sediment was near 1.7 in both cases. Whereas this value was sufficiently large to render the feed poorly sorted and thus allow substantial room for differential mobility, it was still much smaller than the value of 2.59 which characterized the feed sediment in Runs 1–4 of the SAFL fining experiments. The specific gravity of the sediments was close to 2.65. Characteristics of the sediment feed are reported in Table 1; therein D_{f90}, D_{f50}, and D_{f10} denote the sizes in the feed that were 90, 50, and 10% finer, respectively.

The results of 16 experiments are reported here. Twelve of these experiments consist of six pairs of S1/L1–S3/L3 and S1b/L1b–S3b/L3b, with one each (e.g., S1) in the small and large (e.g., L1) flumes. Three more runs were conducted in the small flume (S4–S6), and one more in the large flume (L0), to explore a wider range of conditions. The sediment feed rates Q_{fs} and water discharges Q_w are reported in Table 2, along with the ratio Q_w/Q_{fs}. As can be seen therein, in the case of the paired runs the scale relations associated with Froude similarity, that is

$$(Q_{fs})_S = \lambda^{2.5}(Q_{fs})_L; \quad (Q_w)_S = \lambda^{2.5}(Q_w)_L \tag{4a,b}$$

in which the subscript L denotes large; the subscript S denotes small; and $\lambda = 1/3$ have been satisfied to a reasonable degree of accuracy. The purpose of the four unpaired experiments was to study the deposits associated by relatively large ratios Q_w/Q_{fs}, which in turn created relatively small depositional slopes.

The experimental setup, which is schematized in Fig. 3, was essentially identical to that used in the DSF experiments. The initial bottom of both flumes was a smooth, horizontal, and inerodible fixed bed. A flow of water was commenced, and sediment was introduced at the upstream end from a screw feeder (small flume) or by hand (large flume). The sediment deposit so formed gradually aggraded and prograded downstream. The prograding downstream end of the deposit consisted of an avalanche face advancing into standing water. The average slope of the avalanche face was 39°, indicating that it was at or near the angle of repose θ_r. The standing water,

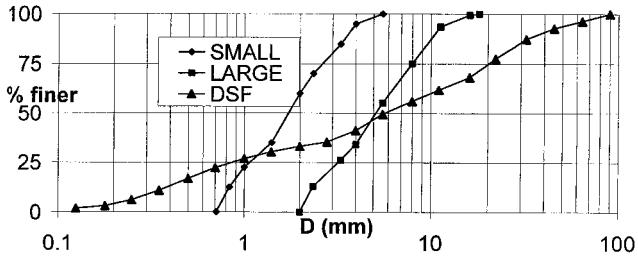

FIG. 2. Grain Size Distributions of Feed Sediments Used in Small and Large Flumes as Well as That for Runs 1–4 of DSF Experiments

TABLE 1. Characteristics of Feed Sediment

Parameter (1)	Small flume (2)	Large flume (3)	DSF Runs 1–4 (4)
D_{fg} (mm)	1.73	5.10	4.44
σ_{fg}	1.71	1.73	6.01
D_{f90} (mm)	3.65	10.49	37.7
D_{f50} (mm)	1.74	5.15	5.75
D_{f10} (mm)	0.81	2.28	0.33

TABLE 2. Characteristic Parameters of Experiments

Run (1)	Q_{fs} (g/s) (2)	Q_w (cm^3/s) (3)	Q_w/Q_{fs} (mass) (4)	t_r (min) (5)	L_d (cm) (6)	Δ_F (cm) (7)	S (8)	H (cm) (9)
S1; L1	6.5; 105	147; 2,384	23; 23	27; 32	120; 296	5.9; 12.5	0.068; 0071	1; 2.5
S2; L2	6.5; 105	432; 7,111	66; 68	23; 40	131; 424	5.7; 11.5	0.037; 0.04	1.8; 4.5
S3; L3	6.5; 105	712; 11,544	110; 110	20; 34	130; 416	5.8; 12	0.03; 0.031	2.6; 6
S1b; L1b	3; 49	147; 2,384	49; 49	34; 60	79; 336	6.5; 14	0.051; 0.055	1; 2.5
S2b; L2b	3; 49	432; 7,111	144; 145	34; 60	85; 398	6.3; 13.7	0.028; 0.029	2; 4.5
S3b; L3b	3; 49	712; 11,544	237; 236	29; 50	80; 310	6; 14.2	0.023; 0.023	3; 6
S4	6.5	1,124	173	21	151	6	0.023	3; 7
S5	6.5	2,273	350	14	92	4.2	0.021	7
S6	3	3,100	1,033	14	64	2.4	0.017	11
L0	12	10,825	902	180	276	14	0.018	7

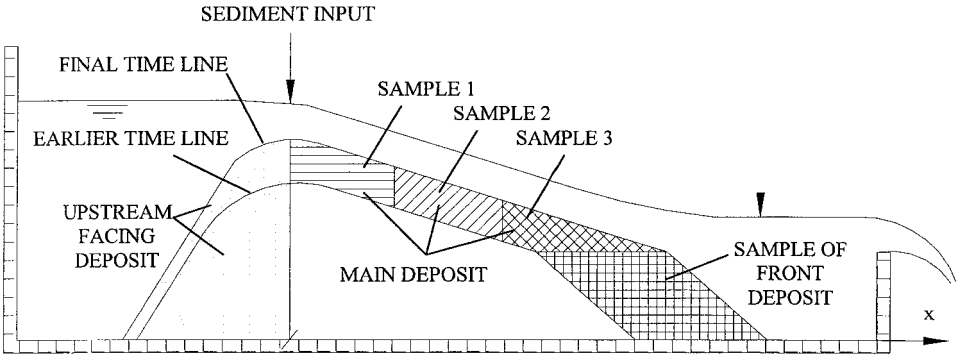

FIG. 3. Schematization of Experimental Setup and Sediment Sampling Procedure

which was maintained by a weir at the downstream end of each flume, determined the height of the progradational front Δ_F. The values for this parameter are listed in Table 2. The average value of Δ_F for the experiments in the small flume is about 0.4 times the average value for the large flume, indicating that the 1:3 scaling is close but not perfect in this parameter.

The duration of each run t_r is listed in Table 2. In all of the paired runs except the pair S1/L1 Froude similarity in run time is satisfied such that

$$(t_r)_S = \lambda^{1/2}(t_r)_L \tag{5}$$

The experiments were terminated before the progradational front had reached the end of the flume, so that steady, uniform equilibrium conditions never developed. In the paired experiments run time was chosen to satisfy Froude similarity. This is because the focus of these experiments was the disequilibrium state in which the deposit was always both aggradational (such that the bed was building up vertically everywhere) and progradational (such that the depositional front was always migrating downstream into standing water). It was hoped that this disequilibrium would provide good conditions for grain sorting according to size. The mode of sediment transport in all of the experiments was observed to be bed load, with intermittent suspension of only the finest sizes in the mix (if at all).

The elevation of the long profile of the deposit was measured from time to time during each run, to provide ''time lines'' describing the top of the deposit. At the end of the run the deposit was sampled between the final time line and a previous time line chosen to allow sufficient deposit thickness, as shown in Fig. 3. By definition the size distribution of all of the sediment between two time lines must be equal to that of the feed sediment.

The full deposit between the two time lines was divided into four sampling zones as described in Fig. 3. The aggradational reach from the feed point to the avalanche front, which defined the main deposit, was divided into three subreaches, yielding the following subsamples: Sample 1 (upstream or proximal), Sample 2 (midstream or medial) and Sample 3 (downstream or distal). The fourth subsample consisted of the material deposited at the avalanche front (i.e., the front sample). As each subsample was taken an estimate of the streamwise distance x of its centroid from the feed point was recorded. The small amount of material that rolled upstream from the feed point to build the upstream end of the deposit (i.e., the upstream-facing deposit of Fig. 3) was not sampled or analyzed. All sediment samples were dried, sieved, and analyzed according to standard methods.

EXPERIMENTAL RESULTS

The two most striking features of the experiments were as follows.

- Straight profiles: The long profiles of the bed were remarkably straight up from the feed point to the avalanche front, displaying virtually none of the upward concavity that typically characterizes aggrading deposits.
- Downstream coarsening: In all but one of the 16 runs the deposit showed downstream coarsening, in most cases quite prominently. Downstream fining was obtained in a single experiment. The pattern of sediment sorting typically became apparent in the first few minutes of the experiment and then was maintained for the duration as the deposit prograded.

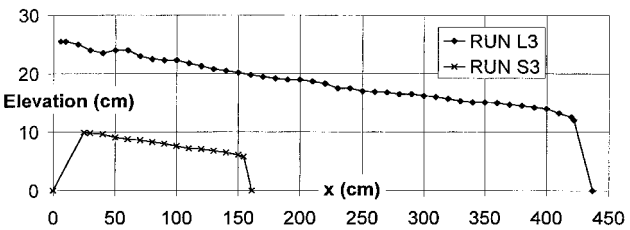

FIG. 4. Final Log Profiles of Bed for Runs S3 and L3

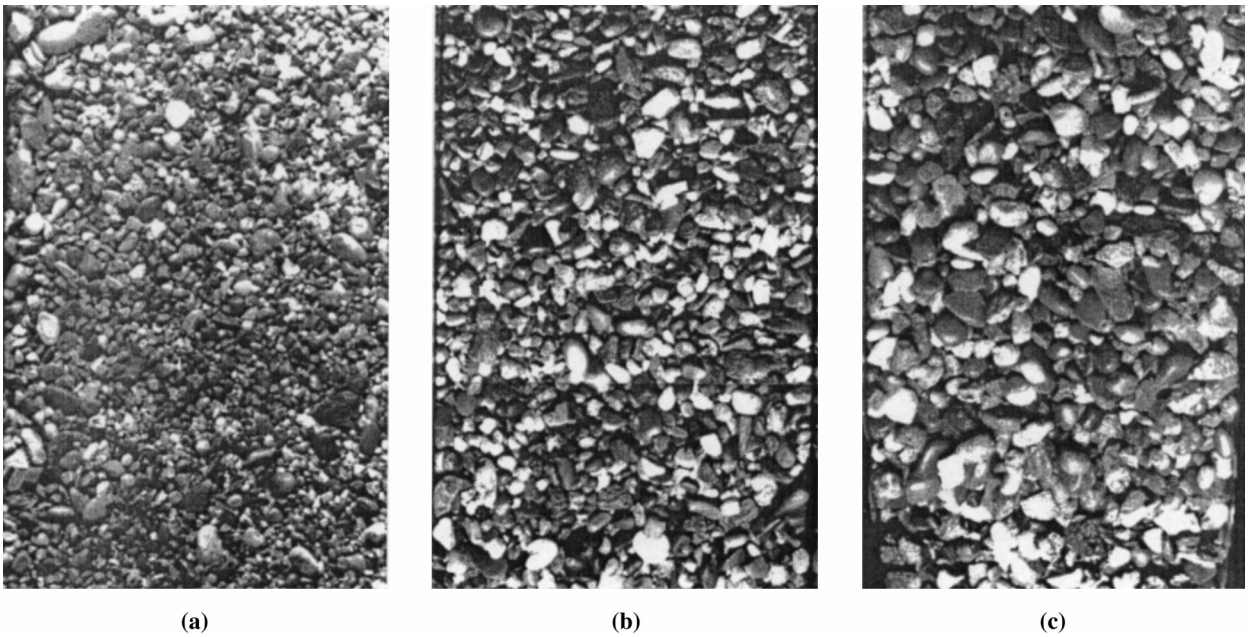

FIG. 5. Photographic Illustration of Downstream Coarsening Seen at End of Run L3: (a) Upstream Sediment Surface at $x^* = 0.16$; (b) Midstream Surface at $x^* = 0.50$; (c) Downstream Surface at $x^* = 0.84$

These features are discussed in more detail below. Runs S3 and L3 are used as the focus of the discussion because they typify the experimental results as a whole.

The following parameters associated with the end of each run are listed in Table 2: length of the main deposit L_d from feed point to the upstream end of the avalanche front, height of the avalanche front Δ_F, mean bed slope of the bed S from the feed point to the avalanche front, and mean flow depth H from the feed point to the avalanche front. Due to the straightness of the long profile from the feed point to the avalanche the listed mean values of S and H also approximate local values over the reach in question.

The long profiles of the bed measured at the end of Runs S3 and L3 are shown in Fig. 4; the lack of concavity is readily apparent. Essentially straight long profiles were observed in all of the experiments. The pattern of downstream coarsening is illustrated clearly in Fig. 5, which shows images of the deposit surface at the same scale for the upstream, midstream, and downstream regions. The streamwise location of the centroid of each photograph is given in dimensionless form as x^*, where

$$x^* = \frac{x}{L_d} \tag{6}$$

It should be noted here that no armor layer at the deposit surface could be distinguished; this obviated separate sampling for both surface and substrate.

Further evidence of the pattern of downstream coarsening is given in Fig. 6, which shows the grain size distributions of the upstream, midstream, and downstream deposits for the paired experiments S3 and L3. Both show strong downstream coarsening. The difference in the pattern of the grain size distributions between the two runs suggests, however, the presence of at least some scale effect.

In Fig. 7 the grain size distribution of the front deposit is compared with that of the feed deposit for Runs S3 and L3. In both cases the front deposit is coarser than the feed deposit, demonstrating the preferential transport of the coarser material to the prograding front. This pattern is further illustrated in Fig. 8, which shows the coarse layer placed at the bottom of the deposit as the front prograded into still water.

Also shown in Fig. 7 are the size distributions obtained from

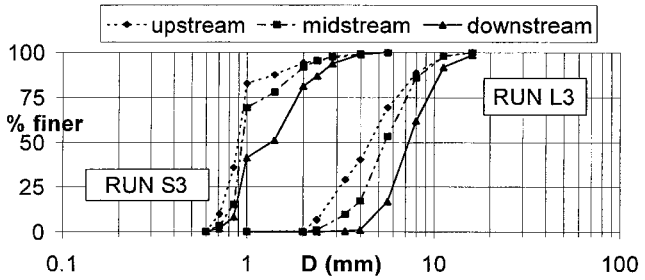

FIG. 6. Grain Size Distributions for Upstream, Midstream, and Downstream Samples Taken at End of Runs S3 and L3

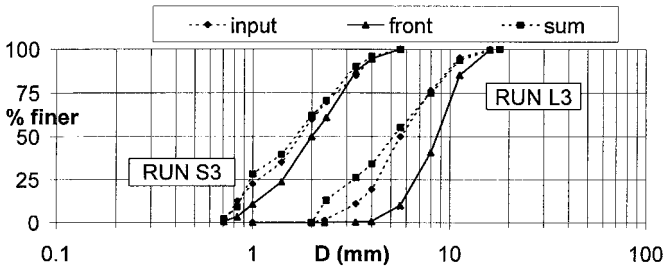

FIG. 7. Grain Size Distributions for Front Samples and Composites of Upstream, Midstream, Downstream, and Front Samples for Runs L3 and S3. Also Shown Are Grain Size Distributions for Feed Sediment

a composition of all four samples for each of Runs L3 and S3. As expected, each composite size distribution is very close to that of the sediment feed, providing a check of sediment continuity. The small difference is mostly attributable to the unsampled upstream-facing deposit of Fig. 3.

In describing further aspects of the pattern of downstream grain size variation it is useful to introduce the logarithmic ψ scale, defined such that

$$D = 2^{\psi}; \quad \psi = \log_2(D) \tag{7a,b}$$

where D = grain size (mm). The geometric mean grain size D_g and geometric standard deviation σ_g, for example, are then related to the arithmetic mean ψ_m and the arithmetic standard deviation σ_ψ, both computed using the ψ scale, by the corresponding relations

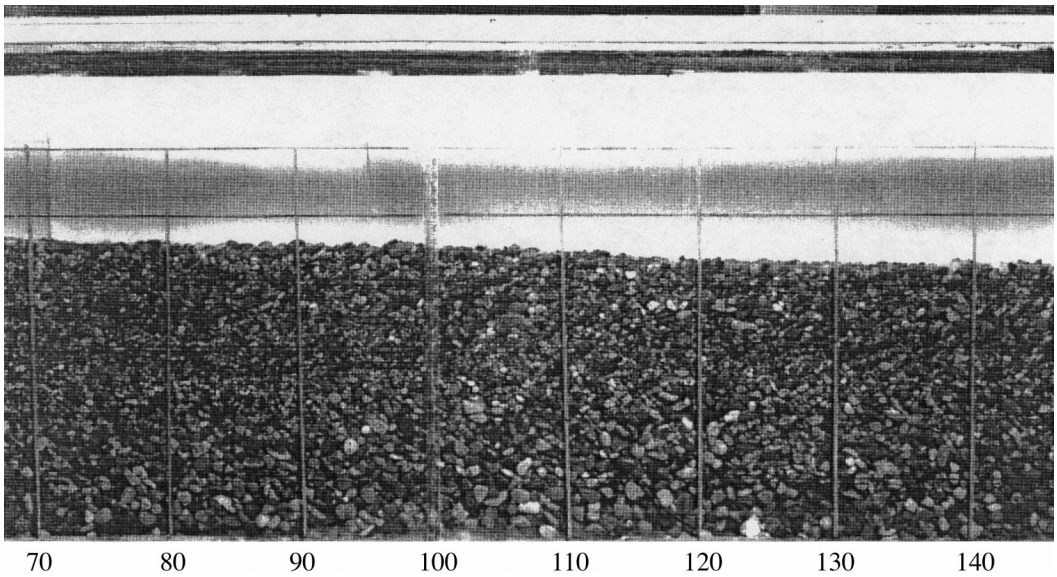

FIG. 8. Photograph Illustrating Coarse Basal Formed during Run L3 Created by Progradation of Deposit Front

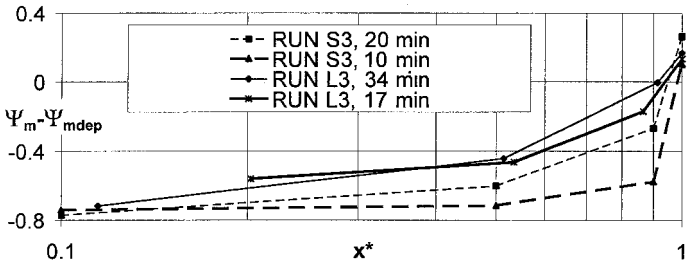

FIG. 9. Plot of $\psi_m - \psi_{mdep}$ versus x^* for Run S3 (10 and 20 min after Commencing Run) and Run L3 (17 and 34 min after Commencing Run)

$$D_g = 2^{\psi_m}; \quad \sigma_g = 2^{\sigma_\psi} \tag{8a,b}$$

Let $\psi_m(x^*)$ denote the mean grain size on the ψ scale at a dimensionless distance x^*, and let ψ_{mdep} denote the corresponding mean grain size of the deposit as a whole (Samples 1–3 and the front sample). Note that ψ_{mdep} provides a good approximation of the mean size ψ_{fm} of the feed material, the difference attributable to the small amount of sediment rolling upstream from the feed point. Fig. 9 shows a plot of the difference $\psi_m(x^*) - \psi_{mdep}$ as a function of x^* for Runs S3 and L3. Results are shown for both the end of each run and at an intermediate time corresponding to about 60% of run time. The pattern of downstream coarsening is shown in terms of the values of $\psi_m(x^*) - \psi_{mdep}$ that are negative upstream and positive downstream. The strength of downstream coarsening increases in the downstream direction, with the front deposits being exceptionally coarse. The pattern of downstream coarsening, when plotted in this dimensionless form, does not appear to vary too strongly with time.

Basic data on the pattern of downstream variation in grain size at the end of each run are given in Table 3; therein x_u^*, x_m^*, x_d^*, x_f^* denote the dimensionless streamwise coordinates of the centroid of Sample 1 (upstream), Sample 2 (midstream), Sample 3 (downstream), and the front sample, respectively, and D_{ug}, D_{mg}, D_{dg}, and D_{fg} denote the geometric mean grain sizes of Sample 1 (upstream), Sample 2 (midstream), Sample 3 (downstream), and the front sample, respectively. Also shown in the table are the geometric mean size D_{depg} and geometric standard deviation σ_{depg} of the composite of the four samples on the ψ scale. Finally, the dimensionless downstream coarsening rate V_g [i.e., the normalized rate of spatial variation of mean grain size on the ψ scale over the main deposit (Samples 1–3)] has been estimated as follows:

TABLE 3. Basic Data on Downstream Variation in Mean Grain Size

Run (1)	D_{ug} (mm) (2)	x_u^* (3)	D_{mg} (mm) (4)	x_m^* (5)	D_{dg} (mm) (6)	x_d^* (7)	D_{fg} (mm) (8)	x_f^* (9)	D_{depg} (mm) (10)	σ_{depg} (11)	V_g (12)
S1	1.14	0.17	1.41	0.50	1.94	0.83	2.41	1	1.66	1.75	1.48
L1	4.06	0.10	5.12	0.51	7.36	0.91	8.10	1	6.16	1.59	1.35
S2	0.89	0.17	1.06	0.50	1.41	0.84	2.19	1	1.66	1.75	1.26
L2	4.06	0.11	5.28	0.50	7.19	0.89	8.25	1	6.54	1.57	1.33
S3	0.96	0.10	1.08	0.50	1.36	0.90	1.97	1	1.64	1.70	0.81
L3	4.52	0.12	5.47	0.51	7.10	0.91	8.27	1	6.74	1.54	1.04
S1b	1.12	0.16	1.22	0.49	1.45	0.84	1.98	1	1.72	1.77	0.70
L1b	4.14	0.10	4.14	0.50	4.74	0.90	6.95	1	5.68	1.67	0.31
S2b	1.01	0.16	1.11	0.52	1.20	0.85	1.84	1	1.64	1.73	0.47
L2b	4.21	0.17	4.80	0.51	5.80	0.84	7.77	1	6.48	1.56	0.87
S3b	1.22	0.16	1.29	0.50	1.41	0.84	1.91	1	1.76	1.70	0.41
L3b	4.26	0.17	4.47	0.50	5.36	0.83	7.16	1	6.43	1.54	0.63
S4	1.00	0.15	1.31	0.53	1.45	0.91	1.99	1	1.74	1.69	0.92
S5	1.60	0.16	1.77	0.50	1.79	0.84	1.75	1	1.74	1.77	0.30
S6	1.58	0.08	1.73	0.50	1.32	0.86	1.69	1	1.74	1.78	−0.43
L0	4.21	0.17	4.08	0.50	4.71	0.83	5.82	1	5.41	1.62	0.31

$$V_g = \frac{1}{\sigma_{f\psi}} \frac{d\psi_m}{dx^*} \cong \frac{1}{\sigma_{f\psi}} \frac{\psi_{dm} - \psi_{um}}{x_d^* - x_u^*} \tag{9}$$

where ψ_{dm}, ψ_{um}, and $\sigma_{f\psi}$ are related to $D_{dg}D_{ug}$, and σ_{fg} in accordance with (7*a*) and (7*b*). Note that a positive value of V_g corresponds to downstream coarsening in the mean size, and a negative value corresponds to downstream fining. Downstream coarsening is seen to have been realized in all runs except one (S6).

REJECTION OF THREE HYPOTHESES FOR DOWNSTREAM COARSENING

In Table 4 values for several dimensionless parameters are listed for the conditions at the end of each run. The flow Reynolds number R, Froude number F, and Shields stress based on geometric mean sediment size of the feed sediment τ_{fg}^* are given by the relations

$$\mathsf{R} = \frac{UH}{\nu}; \quad \mathsf{F} = \frac{U}{\sqrt{gH}}; \quad \tau_{fg}^* = \frac{r_b S}{\left(\frac{\rho_s}{\rho} - 1\right) D_{fg}} \tag{10a–c}$$

In the above relations U denotes cross-sectionally averaged flow velocity; g denotes the acceleration of gravity; ν denotes the kinematic viscosity of water; ρ denotes water density; and

TABLE 4. Dimensionless Parameters Associated with Experiments

Run (1)	R (2)	F (3)	τ^*_{fg} (4)	δ_{bv}/k_{sf} (5)	δ_{bv}/D_{f10} (6)	H/D_{f90} (7)
S1; L1	2,940; 15,890	0.94; 1.28	0.19; 0.18	0.0217; 0.0046	0.098; 0.021	2.74; 2.38
S2; L2	8,640; 47,410	1.14; 1.59	0.15; 0.15	0.0246; 0.0050	0.111; 0.023	4.93; 4.29
S3; L3	14,240; 76,960	1.08; 1.67	0.13; 0.13	0.0262, 0.0053	0.118; 0.024	7.12; 5.72
S1b; L1b	2,940; 15,890	0.94; 1.28	0.14; 0.14	0.0251; 0.0052	0.114; 0.024	2.74; 2.38
S2b; L2b	8,640; 47,410	0.98; 1.59	0.12; 0.11	0.0277; 0.0058	0.125; 0.027	5.48; 4.29
S3b; L3b	14,240; 76,960	0.87; 1.67	0.10; 0.10	0.0299; 0.0061	0.135; 0.028	8.22; 5.72
S4	22,480	1.01	0.10	0.0299	0.135	10.14
S5	45,460	0.78	0.09	0.0313	0.142	19.19
S6	62,000	0.54	0.07	0.0348	0.157	30.15
L0	72,170	1.24	0.08	0.0068	0.031	6.67

ρ_s denotes sediment density. In addition r_b denotes the hydraulic radius of the bed region of the channel cross section, as defined below. All Reynolds numbers are in the turbulent range. In some of the experiments in the small flume, however, the turbulence may have been rather coarse. It is also seen that perfect Froude similarity was not satisfied between the paired runs in the small and large flumes. The Froude number tended to be somewhat smaller in the small flume than in the large flume. This is probably the result of some residual viscous effects in the small flume. The Froude numbers cover the range from subcritical to well into the supercritical range. The Shields stresses τ^*_{fg} generally argue for active bed-load transport, as was actually observed in the experiments.

The dimensionless ratios δ_{bv}/k_{sf}, δ_{bv}/D_{f10}, and H/D_{f90} are shown in Table 4. Here k_{sf} denotes an estimate of the roughness height of the deposit based on sediment feed characteristics; it is here taken to be equal to $2D_{f90}$. In addition δ_{bv} is an estimate of the viscous length scale based solely on bed properties. It was necessary to introduce this parameter because the depth-to-width ratio H/B in the experiments tended to be large, so that much of the resistance was exerted against the walls instead of the bed. A standard method of decomposition of boundary shear stress between wall and bed in flumes can be found in Vanoni (1975). Following that analysis, it is assumed here that

$$\delta_{bv} = 11.6\,\frac{\nu}{u_{*b}}; \quad u_{*b} = \sqrt{g r_b S} \tag{11a,b}$$

$$r_b = \begin{cases} \dfrac{B}{4} & \text{for} \quad H > \dfrac{B}{2} \\ \dfrac{1}{B}\,[H^2 + H(B - 2H)] & \text{for} \quad H < \dfrac{B}{2} \end{cases} \tag{11c}$$

in the above relations u_{*b} denotes a bed-shear velocity.

One of the hypotheses for downstream coarsening can be immediately rejected as the cause of the phenomenon in the case of the present experiments. The feed sediment, although poorly sorted, showed no obvious bimodality, as can be seen in Fig. 2. Bimodality thus cannot be invoked as the cause of the observed downstream coarsening.

Bimodality did, however, play a role in all of the experiments in the small flume, as is evident from the data pertaining to Run S3 in Figs. 6 and 7. Sediment ranging from 1 to 1.41 mm constituted 12.5% of the feed sediment, but by the end of the run constituted only 4.8% of the upstream Sample 1, 8.6% of the midstream Sample 2, and 9.9% of the downstream Sample 3. The result is the evolution of a noticeable bimodality, particularly in the upstream half of the flume, with content in the ranges of 0.6–1 mm and 1.4–5.6 mm and an intervening range of relatively little content. Sediment in the range of 1–1.41 mm constituted 13.1% of the sediment in the front sample, and 11.3% of the composite of the four samples. Evidently this size range of 1–1.41 mm was preferentially transported to the downstream end of the deposit.

Whatever the cause of this phenomenon in the small flume, however, it cannot be invoked as the explanation for downstream coarsening. This is because the geometric mean size of the range in question is 1.19 mm (i.e., substantially finer than the geometric mean size of the feed sediment). The self-evolving bimodality evident in the experiments in the small flume thus acted to suppress, not amplify, the observed downstream coarsening. It should be noted that a similar tendency for self-evolving bimodality was not observed in the large flume.

A second hypothesis, namely, flow blocking effects, can be similarly rejected. The observed values of H/D_{f90} are given in Table 4. Among the runs evincing downstream coarsening (all but one), this parameter varies from 2.4 to 19.2. In Runs 1–3 of the DSF experiments (all of which evinced downstream fining) this parameter fell in the range of 3.5–5 (i.e., in the range corresponding to the strongest downstream coarsening observed in the present experiments).

Finally, the hypothesis of viscous effects can be conclusively rejected. As can be seen from Table 4, the parameter δ_{bv}/k_{sf} was never larger than 0.007 in the large flume and never larger than 0.035 in the small flume. Any residual viscous sublayer must be extremely limited in the small flume and essentially absent in the large flume. The parameter δ_{bv}/D_{f10} in Table 4 is seen to never have exceeded 0.16 in the small flume and 0.031 in the large flume. Thus even if a residual viscous sublayer did exist it would have been insufficient to protect even grains as fine as D_{f10} from the turbulent flow above. Although weak viscous effects may have been a factor in the self-evolving bimodality in the small flume, which hindered rather than strengthened the observed downstream coarsening, they can be expected to have been entirely absent in the large flume. Thus downstream coarsening can occur in the absence of viscous effects.

WHAT CAUSES DOWNSTREAM COARSENING?

In the coarse of the experiments it became apparent that downstream coarsening tended to be most prominent at the highest bed slopes, which were in turn correlated with the

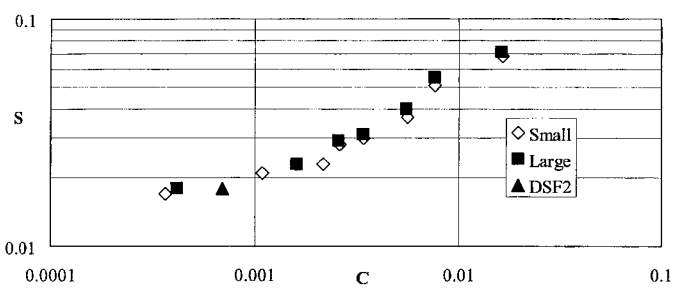

FIG. 10. Plot of Deposit Slope *S* versus Volume Sediment Concentration *C* at Feed Point

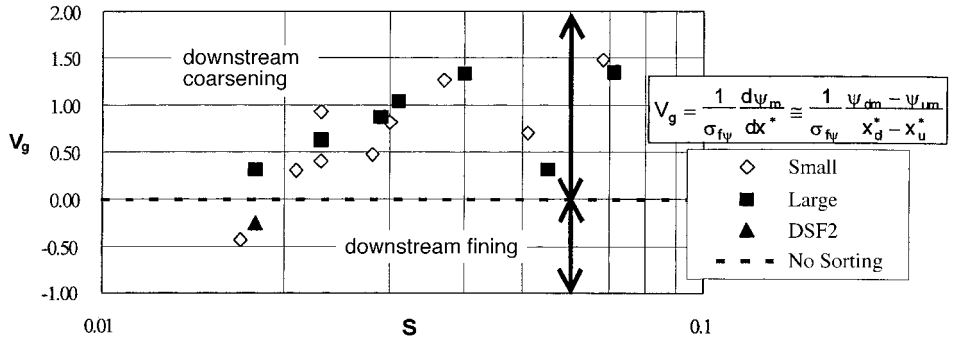

FIG. 11. Plot of Dimensionless Downstream Rate of Variation of Mean Size V_g versus Deposit Slope S

highest sediment feed concentrations. In Fig. 10 final slope S of the main deposit (between the feed point and the upstream end of the front) is plotted against the volume concentration C of the sediment in the feed, which is given by the following relation:

$$C = \frac{Q_{fs}/(\rho_s/\rho)}{Q_{fs}/(\rho_s/\rho) + Q_w} \tag{12}$$

Included in the plot are values for Run 2 of the DSF experiments reported in Seal et al. (1997) and referred to as Run DSF2 below; very similar results were obtained for Runs 1 and 3. In the case of Run DSF2, the slope represents an average value over a mildly upward concave profile. A strong correlation between sediment concentration and slope is evident. Only three experiments had slopes below 0.02—Run S6, Run L0, and Run DSF2. Of these runs, Runs S6 and DSF2 evinced downstream fining, and Run L0 was tied with another run for the weakest downstream coarsening of the runs in the large flume.

The dimensionless rate of downstream variation in grain size V_g computed from (9) is plotted against deposit slope in Fig. 11. Data for Run DSF2 were obtained from Seal et al. (1997, Tables 1 and 3); here x_u = 3 m, x_d = 24 m, and L_d = 36.8 m. The plot provides strong evidence that downstream coarsening is due to a slope effect, with a mobility reversal occurring for slopes in excess of a value in the neighborhood of 0.02–0.03.

Only two experiments in Fig. 11 show downstream fining [i.e., Run S6 of the present set and Run DSF2 of Seal et al. (1997)]. Two more experiments evincing downstream fining [i.e., those pertaining to Runs DSF1 and DSF3 of Seal et al. (1997)] are also available; they are not shown in Fig. 11 because the average bed slopes differ little from that of Run DSF2.

WHY SHOULD INCREASING SLOPE CAUSE A MOBILITY REVERSAL?

Evidence that a mobility reversal might occur at sufficiently steep slopes is provided by talus deposits of rock debris at the base of slopes. Such deposits are typically near the angle of repose. In addition, they often display a prominent downslope coarsening in their deposits. The origin of this sorting is reasonably clear; in a poorly sorted granular material on a steep, dry slope the finer grains display a higher friction angle than coarser grains [e.g., Miller and Byrne (1966)].

It is not obvious, on the other hand, why a mobility reversal should occur at a slope between 0.02 and 0.03—values that are an order of magnitude lower than any reasonable value for the slope corresponding to the angle of repose for granular material. A first attempt at an explanation is given here.

The basis for the analysis are the treatments of Ikeda (1982), Parker and Andrews (1985), and Kovacs and Parker (1994). A direct slope effect on the critical shear stress for granular material subjected to the flow of water has been recognized for several decades. For example, Kovacs and Parker (1994) noted that the relation for the critical Shields stress must be modified accordingly for sufficiently large bed slope

$$\frac{\tau_c^*}{\tau_{c0}^*} = \left(1 - \frac{S}{\mu}\right) \cos\theta \tag{13}$$

where τ_c^* denotes the critical Shields stress for the onset of motion; τ_{c0}^* denotes the corresponding value on a negligible slope S; θ denotes the angle of inclination of the bed so that S equals $\tan\theta$; and μ denotes the Coulomb friction coefficient of the sediment, which is related to the angle of repose θ_r as

$$\mu = \tan\theta_r \tag{14}$$

The above relation, which applies to sediment with a uniform size, predicts that the critical Shields stress drops to zero when the slope becomes equal to that corresponding to the angle of repose, or friction angle. At a slope as low as 0.03, however, the equation predicts only a 3.7% reduction in critical Shields stress at a friction angle of 39°.

In the analysis that follows below, D denotes grain size, D_g specifically refers to the geometric mean size of sediment exposed to the flow at the surface (i.e., geometric mean of the active or exchange layer), and θ denotes the slope angle of the bed, such that

$$S = \tan\theta \tag{15}$$

Consider a grain of size D within a mixture of grain sizes exposed at the bed surface, as shown in Fig. 12. The tangential (streamwise) and normal gravitational forces F_{Gt} and F_{Gn} acting on the particle are given by

$$F_{Gt} = \rho R \frac{4}{3} \pi \left(\frac{D}{2}\right)^3 g \sin\theta \tag{16a}$$

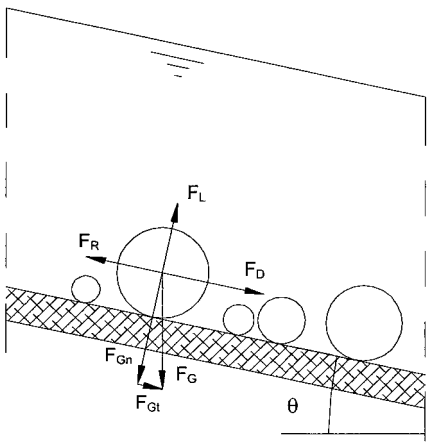

FIG. 12. Schematic Diagram Illustrating Forces on Grain Exposed on Bed Surface

$$F_{Gn} = \rho R \frac{4}{3} \pi \left(\frac{D}{2}\right)^3 g \cos \theta \tag{16b}$$

where

$$R = \frac{\rho_s}{\rho} - 1 \tag{17}$$

The lift and drag forces operating on the particle F_D and F_L are given by

$$F_D = \rho c_D \frac{1}{2} \pi \left(\frac{D}{2}\right)^2 u_p^2; \quad F_L = \rho c_L \frac{1}{2} \pi \left(\frac{D}{2}\right)^2 u_p^2 \tag{18a,b}$$

where c_D denotes a drag coefficient; c_L denotes a lift coefficient; and u_p = effective velocity acting on the grain, related to the shear velocity u_* and boundary shear stress τ_b as

$$\frac{u_p}{u_*} = F_u; \quad \tau_b = \rho u_*^2 \tag{19a,b}$$

Although the values of c_D, c_L, and F_u can be expected to differ randomly from particle to particle due to random placement, on average they can be expected to be a function of grain size D. The resistive force opposing motion is given by

$$F_R = \mu(F_{Gn} - F_L) \tag{20}$$

where again μ can be expected to be a function of grain size D.

The critical condition for the threshold of motion is given by the force balance

$$F_D + F_{Gt} = F_R \tag{21}$$

Upon reduction of (21) with (16)–(21) it is found that the critical Shields stress for the onset of particle motion is given by

$$\tau_c^* = \frac{\tau_{bc}}{\rho R g D} = \frac{4\mu \cos \theta}{3F_u^2(c_D + \mu c_L)} \left(1 - \frac{S}{\mu}\right) \tag{22}$$

where τ_{bc} denotes the critical boundary shear stress for the motion of a particle of size D. Now let τ_{bgc} denote the critical boundary shear stress for the motion of the geometric mean size D_g. Eq. (22) then reduces to the form

$$\frac{\tau_{bc}}{\tau_{bgc}} = R_H R_S; \quad R_H = \frac{D}{D_g} \frac{\mu}{\mu_g} \left(\frac{F_{ug}}{F_u}\right)^2 \frac{c_{Dg} + \mu_g c_{Lg}}{c_D + \mu c_L} = R_H(r) \tag{23a,b}$$

$$R_S = \frac{\mu_g}{\mu} \left(\frac{\frac{\mu}{\mu_g} - \frac{S}{\mu_g}}{1 - \frac{S}{\mu_g}} \right) = R_S(r, S); \quad r = \frac{D}{D_g} \tag{23c,d}$$

In the above relations the subscript g on c_D, c_L, and μ denote values evaluated for size D_g. Thus by definition both R_H and R_S must equal unity at $r = 1$ ($D = D_g$).

It is seen from the above equations that the slope effect enters the analysis only through the term R_S. The term R_H expresses the variation of critical boundary shear stress with size for horizontal beds and beds with slopes that are sufficiently small to allow for the neglect of slope. In developing a surface-based sediment transport relation based mostly on field data from Oak Creek, Oreg., Parker (1990) obtained the empirical power relation

$$R_H = r^{\delta_H} \tag{24}$$

where δ_H is close to 0.1. Such a relation, which renders coarser grains exposed on the surface somewhat less mobile (due to a higher value of τ_c) than their finer neighbors, is the basis for the predictions of downstream fining due to selective transport under aggradational and progradational conditions described in Parker (1991a,b), Cui et al. (1996), and Cui and Parker (1998). In particular, the analysis of Cui et al. (1996) provides a reasonable description of the patterns of downstream fining observed in DSF Runs 1–3 (Seal et al. 1997).

The positive but relatively low value of the exponent δ_H appears to be dedicated by a competition between downward normal gravitational and hiding effects. In particular, particle weight increases with the cube of grain size, making larger grains much more difficult to move than their finer siblings (at low values of S). This is in turn almost completely balanced by a variety of hiding effects, according to which finer grains on the average protrude out from the bed to a lesser degree than coarser grains, and thus feel reduced drag and lift and increased frictional resistance to mobilization. The residual mobility increase of coarser grains is thus modest but sufficient to drive observed patterns of downstream fining.

The value of δ_H of about 0.1 determined from the Oak Creek data may, however, already contain some slope effect. This is because the slope of Oak Creek near the sediment sampling site is 0.01. With this in mind, the following somewhat larger value of δ_H is used below and justified a posteriori by matching with the Oak Creek exponent of 0.1:

$$\delta_H = 0.12 \tag{25}$$

The following simple power law is assumed for the variation of Coulomb friction coefficient with grain size:

$$\frac{\mu}{\mu_g} = r^{-\delta_R} \tag{26}$$

where δ_R is taken to be positive; and the minus sign in the exponent indicates that coarser grains are expected to have a lower friction coefficient than finer grains. Substituting (24) and (26) into (23*a*) and (23*c*), it is found that

$$\frac{\tau_{bc}}{\tau_{bgc}} = r^{\delta_H + \delta_R} \frac{r^{-\delta_R} - \frac{S}{\mu_g}}{1 - \frac{S}{\mu_g}} \tag{27}$$

Here the problem of mobility reversal is approached in a simple empirical way; a value of δ_R is sought that yields the observed behavior. The friction angle extracted from an extrapolation of mobile-bed conditions to the threshold of motion can be expected to be somewhat smaller than the static value [e.g., Ashida and Michiue (1972)]. With this in mind, a value of μ_g of 0.5, corresponding to a friction angle of 26.6°, is employed here. The value of δ_R was selected by trial and error to yield a functional relationship close to (24) with $\delta_H = 0.1$ at $S = 0.01$ and a mobility reversal for values of S between 0.02 and 0.03. The result was a value of δ_R of 0.9.

In Fig. 13, (27) is evaluated with the values $\delta_H = 0.12$, δ_R

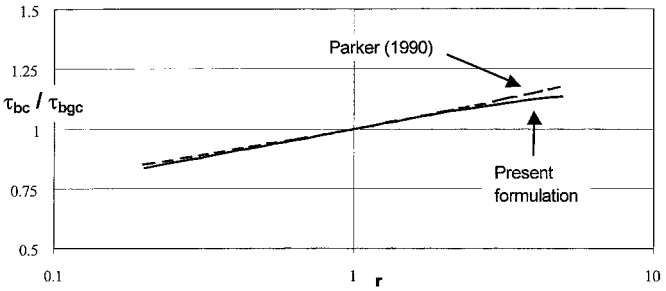

FIG. 13. Comparison of Predicted Mobility Ratio τ_{bc}/τ_{bgc} as Function of Grain Size Ratio at $S = 0.01$ with Mobility Ratio of Parker (1990) Gravel Transport Relation

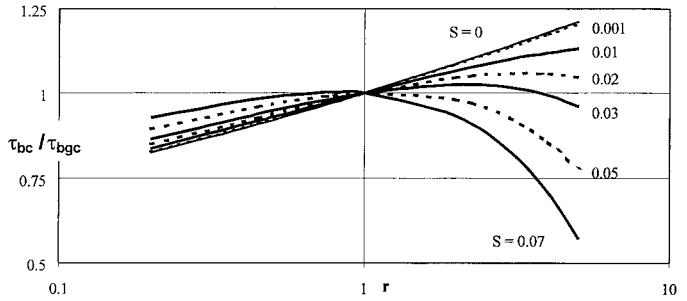

FIG. 14. Illustration of Variation of Mobility Ratio τ_{bc}/τ_{bgc} as Function of Grain Size Ratio r and Bed Slope S. Parameters Associated with Calculation Are Given in Text

= 0.9, μ_g = 0.5, and S = 0.01 and compared with the Oak Creek relationship [(24)] with δ_H = 0.1. The plot indicates that (27) can indeed reproduce the observed functional relationship in Oak Creek.

In Fig. 14, (27) is evaluated using the same parameters as above, except that slope S is allowed to vary from 0 to 0.07 (i.e., near the highest depositional slope in the experiments reported here). At S = 0.001 the slope effect is seen to be negligible. At S = 0.01 no reversal of mobility is observed, but the difference in mobility between coarser and finer grains is somewhat suppressed. At S = 0.02 a slight mobility reversal has appeared, but only in the coarsest grains; the size equal to $5D_g$ has a lower critical shear stress than the size equal to $4D_g$. At S = 0.03 the coarsest sizes are more mobile than some sizes below D_g. At S = 0.07 the mobility pattern is completely reversed, with all grains coarser than D_g rendered more mobile than D_g.

The above combination of theory and empiricism paints the following picture of mobility reversal. On nearly horizontal beds the competition between downward normal gravitational and hiding effects renders finer grains exposed on the surface only somewhat more mobile than their coarser neighbors. The balance is sufficiently delicate that it can be reversed by a relatively small streamwise tangential gravitational effect. The phenomenon of mobility reversal is mediated by a variation in Coulomb friction coefficient with grain size that substantially reduces the coefficient for coarse grains.

The above explanation for the mobility reversal, although appealing, is not immune to criticism. Laboratory measurements of friction angle for sediment mixtures suggest a relation of the form

$$\frac{\theta_f}{\theta_{fg}} = r^{-0.3} \tag{28}$$

where θ_f denotes friction angle and θ_{fg} denotes the value associated with D_g [e.g., Miller and Byrne (1966), Wiberg and Smith (1987), Kirchner et al. (1990)]. If the above relation is converted from angle to Coulomb friction coefficient using a θ_{fg} value of 0.5 and a power law is fitted to the form of (26) over the range of $0.2 \leq r \leq 5$, a somewhat larger δ_R value of 0.35 is obtained. There are three possible explanations for the discrepancy:

- Relations for the variation of friction angle with grain size determined from tilted tables may not apply to slopes well below the angle of repose, where the particles may arrange themselves differently due to the effects of fluid force.
- The above analysis has the right structure but would predict better results with less discrepancy if formulated in terms of torque [e.g., White (1940)]. The implication is that a combination of fluid forces and streamwise gravitational effects would make it much easier to torque out a coarse grain from the bed than a fine grain.
- The above analysis is wrong, and an alternative explanation must be sought.

Recent results due to Johnston et al. (1998) suggest that the first of these may be the correct explanation. The writers overcame the limitations of tilted tables by measuring particle friction angles in situ in five reaches of natural rivers. In two of these cases (i.e., Sagehen Creek and the Van Duzen River), the variation of friction angle with grain size is supportive of the present formulation. Their data allow the determination of estimates of δ_R from regressions of μ versus D/D_{50}. If all the points are used, δ_R values of 0.730 and 0.823 are found for Sagehen Creek and the Van Duzen River, respectively. If only points such that $D/D_{50} > 1$ are included in the regression, these respective numbers increase to 1.16 and 0.980.

CONSEQUENCES OF TIME INVARIANCY OF DEPOSITIONAL SLOPE

The experiments reported here showed depositional slopes S between the feed point and the upstream end of the front that were essentially constant not only in space but in time as well. In all experiments except one (Run L0), S was determined at three times during the course of the runs and found to show little variation. This constancy of depositional slope allows for a very simple model of front propagation. Referring to Fig. 3, the following statement of mass balance can be made:

$$(1 - \lambda_p)\frac{d}{dt}\left[\Delta_F L_d + \frac{1}{2}SL_d^2 + \frac{1}{2}\frac{\Delta_F^2}{\tan\theta_r} + \frac{1}{2}\frac{(\Delta_F + SL_d)^2}{\tan\theta_r}\right] = q_{fs} \tag{29}$$

where λ_p denotes the porosity of the deposit; θ_r denotes the angle of repose of the sediment; and q_{fs} denotes the volume feed rate of sediment, which is in turn equal to $Q_{fs}/(B\rho_s)$. In the above relation the first term within the brackets denotes the volume of the main deposit up to the height of the front, the second term denotes the volume of the main deposit above the top of the prograding front, the third term denotes the volume of sediment in the front, and the fourth term denotes the volume of the deposit upstream of the feed point. The parameter q_{fs} was held constant, and the parameter θ_r was observed to be nearly constant at 3°. The parameters Δ_F and S varied from run to run but were observed to be nearly constant during any particular run.

Further assuming a constant value of deposit porosity λ_p and reducing (29) with these observations, it is found that

$$\left(1 + S\frac{L_d}{\Delta_F}\right)\frac{dL_d}{dt} = \frac{q_{fs}}{(1 - \lambda_p)\left(1 + \dfrac{S}{\tan\theta_r}\right)\Delta_F} \tag{30}$$

The above equation is easily solved for L_d. Because the geometry of Fig. 3 is not likely to be valid in the early stages of deposit formation, the above equation is solved subject to the boundary condition of a known deposit length L_{d0} at some time t_0. In dimensionless form it is found that

$$\hat{L} = \frac{-1 + \sqrt{1 + 2S(\hat{t} - \hat{t}_0) + 2S\hat{L}_0 + S^2\hat{L}_0^2}}{S} \tag{31}$$

where

$$\hat{L} = \frac{L_d}{\Delta_F}; \quad \hat{t} = \frac{q_{fs}}{(1 - \lambda_p)\left[1 + \dfrac{S}{\tan\theta_r}\right]\Delta_F^2}\,t \tag{32a,b}$$

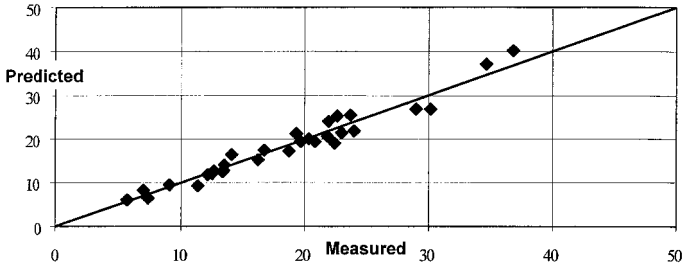

FIG. 15. Plot of Measured versus Predicted Values of Dimensionless Deposit Length $\hat{L}$

In Fig. 15 values of $\hat{L}$ predicted from (31) are compared against observed values for all runs except Run S6, for which data were lacking. To perform the analysis, the initial values $\hat{L}_0$ and $\hat{t}_0$ were obtained from the first profile measured for each run. Eq. (31) was then used to predict $\hat{L}$ for the two later profiles. A value of deposit porosity λ_p of 0.4 was used in the calculations. Excellent agreement between observed and predicted values can be seen in Fig. 15. This justifies the assumption of a spatially and temporally constant depositional slope that is maintained for the duration of each run.

The above analysis, although clearly illustrating a property of the experiments reported here, is not yet predictive because no generally valid equation is available for predicting S as a function of other properties (e.g., water discharge and sediment transport). A first version of the sediment transport relation required for implementing this could, however, be developed with the data obtained in the present study.

CONCLUSIONS

The analysis presented here demonstrates a mobility reversal in sediment mixtures when streamwise bed slope is higher than approximately 0.02. The mobility reversal renders coarser grains somewhat more mobile than fine grains in a mixture, with the result that an aggrading or prograding deposit shows a tendency for downstream coarsening rather than fining in the geometric mean size of the deposit.

The analysis suggests that the mobility reversal is due to the direct effect of gravity acting on sediment grains. This effect, which allows coarse particles to be preferentially plucked from a granular surface, is the cause of the downstream coarsening familiarly observed in grain flows on talus faces. The direct gravitational effect on a granular bed under flowing water with a slope as low as 0.02 is quite weak. This notwithstanding, it appears to be sufficient to disrupt the rather delicate balance between particle weight and hiding effects that renders finer grains exposed at a surface somewhat more mobile than their coarser neighbors at lower slopes. It may turn out that this reversal is ultimately aided (or possibly suppressed) in some cases by bimodality, viscous effects, or flow blocking effects. With this in mind, one may speculate that the precise slope at which the reversal occurs may be a function of these subsidiary factors, as well as the grain size distribution of the sediment load. The experiments reported here demonstrate, however, that the mobility reversal can occur in the absence of any of such subsidiary factors.

This mobility reversal may not be seen in nature very often, because at slopes in excess of 0.02 extremely high rates of continuous sediment supply are necessary to maintain a truly alluvial bed. At such high slopes it is more common for the bed to be activated briefly by, for example, large sediment inputs from debris flows and then quickly erode back during floods to a quasi-static step-pool morphology. This notwithstanding, the writers predict with some confidence that the reversal will indeed be observed in nature under the right conditions.

The present analysis suggests several pitfalls and an avenue for future research. One pitfall concerns distorted Froude modeling, according to which Froude similarity is satisfied but the vertical geometric scale ratio differs from the horizontal scale ratio in such a way that modal slopes are steeper than the prototype. Although the basis for distorted Froude modeling is generally sound, too much exaggeration of the slope in a mobile-bed model can lead to a mobility reversal, and thus unrealistic results in regard to the pattern of grain size variation. This appears to have been the case for the work reported by Straub (1935).

A second pitfall concerns sediment transport equations for mixtures, for which the slope effect described here is generally not included. The gravel transport relation of Parker (1990), for example, depends heavily on field data from a reach of Oak Creek, Oreg., which has a slope of 0.01. It may be that this slope is low enough to prevent a mobility reversal but high enough to moderate the selective transport of finer grains. It is thus possible that the relation systematically underpredicts selective transport of finer grains at much lower slopes.

This second pitfall also offers a research opportunity. Inclusion of the direct gravitational effect on sediment grains in the context of the saltation-based bed-load transport models of Wiberg and Smith (1985) and Sekine and Kikkawa (1992) offers an avenue for a more complete understanding of the effect of slope on mobility reversal.

ACKNOWLEDGMENTS

This research was motivated by coffee-table discussions between Chris Paola and the second writer over many years. John Ahern documented downstream coarsening in a model alluvial fan deposit in the course of an experiment suggested by Chris Paola. In a failed attempt to reproduce a step-pool topography, Kazuo Taki and the second writer accidentally produced downstream coarsening in the small flume used for the present experiments. Grace Chang then went on to conduct a preliminary set of experiments on downstream coarsening what formed the basis for the design of the present experiments. Syunsuke Ikeda offered facilities and support at Tokyo Institute of Technology, Japan, in order to complete this work. This research was funded by the National Science Foundation (Grant No. CTS-9424507).

APPENDIX I. REFERENCES

Ashida, K., and Michiue, M. (1972). ''Basic study on hydraulic resistance and bedload transport in mobile bed flows.'' *Proc., JSCE*, Tokyo, 206, 59–69 (in Japanese).

Cui, Y., and Parker, G. (1998). ''The arrested gravel front: Stable gravel-sand transitions in rivers. Part 2: General numerical solution.'' *J. Hydr. Res.*, Delft, The Netherlands, 36(2), 159–182.

Cui, Y., Parker, G., and Paola, C. (1996). ''Numerical simulation of aggradation and downstream fining.'' *J. Hydr. Res.*, Delft, The Netherlands, 34(2), 185–204.

Egiazaroff, I. V. (1965). ''Calculation of nonuniform sediment concentrations.'' *J. Hydr. Div.*, ASCE, 91(4), 225–247.

Einstein, H. A. (1950). ''Formulas for the transportation of bed-load.'' *Tech. Bull. 1026*, U.S. Department of Agriculture, Soil Conservation Service.

Ikeda, S. (1982). ''Incipient motion of sand particles on side slopes.'' *J. Hydr. Div.*, ASCE, 108(1), 95–114.

Johnston, C. E., Andrews, E. D., and Pitlick, J. (1998). ''In situ determination of particle friction angles of fluvial gravels.'' *Water Resour. Res.*, 34(8), 2017–2030.

Kirchner, J. W., Dietrich, W. E., Iseya, F., and Ikeda, H. (1990). ''Shear stress distributions of water-worked beds.'' *Sedimentology*, 37, 647–672.

Kodama, Y., Ikeda, H., and Iijima, H. (1992). ''Longitudinal sediment sorting along a concave upward stream profile in a large flume.'' *Rep. of the Hydr. Experimental Ctr.*, 16, 119–123 (in Japanese).

Kovacs, A., and Parker, G. (1994). ''A new vectorial bedload formulation and its application to the time evolution of straight river channels.'' *J. Fluid Mech.*, Cambridge, U.K., 267, 153–183.

Miller, R. L., and Byrne, R. J. (1966). ''The angle of repose for a single grain on a fixed bed.'' *Sedimentology*, 6, 303–314.

Paola, C., Heller, P. L., and Angevine, C. L. (1992a). ''The large-scale

dynamics of grain-size variation in alluvial basins. I: Theory.'' *Basin Res.*, 4, 73–90.
Paola, C., Parker, G., Seal, R., Sinha, S. K., Southard, J. B., and Wilcock, P. R. (1992b). ''Downstream finding by selective deposition in a laboratory flume.'' *Sci.*, 258, 1757–1760.
Parker, G. (1990). ''Surface-based bedload transport relation for gravel rivers.'' *J. Hydr. Res.*, Delft, The Netherlands, 20(4), 417–436.
Parker, G. (1991a). ''Selective sorting and abrasion of river gravel. I: Theory.'' *J. Hydr. Engrg.*, ASCE, 117(2), 131–149.
Parker, G. (1991b). ''Selective sorting and abrasion of river gravel. II: Applications.'' *J. Hydr. Engrg.*, ASCE, 117(2), 150–171.
Parker, G., and Andrews, E. D. (1985). ''Sorting of bed load sediment by flow in meander bends.'' *Water Resour. Res.*, 21(9), 1361–1373.
Parker, G., and Cui, Y. (1998). ''The arrested gravel front: Stable gravel-sand transitions in rivers. Part 1: Simplified analytical solution.'' *J. Hydr. Res.*, Delft, The Netherlands, 36(1), 75–100.
Pizzuto, J. (1995). ''Downstream fining in a network of gravel rivers.'' *Water Resour. Res.*, 31, 753–759.
Sambrook Smith, G. H., and Ferguson, R. I. (1995). ''The gravel-sand transition along river channels.'' *J. Sedimentary Res.*, A65(2), 423–430.
Schlichting, H. (1968). *Boundary layer theory.* McGraw-Hill, New York.
Seal, R., Paola, C., Parker, G., Southard, J. B., and Wilcox, P. R. (1997). ''Experiments on downstream fining of gravel: I. Narrow-channel runs.'' *J. Hydr. Engrg.*, ASCE, 123(10), 874–884.
Sekine, M., and Kikkawa, H. (1992). ''Mechanics of saltating grains. II.'' *J. Hydr. Engrg.*, ASCE, 118(4), 536–558.
Shaw, J., and Kellerhals, R. (1982). ''The composition of recent alluvial gravels in Alberta river beds.'' *Bull. 41*, Alberta Research Council, Edmonton, Alta., Canada.
Straub, L. G. (1935). ''Some observations of sorting of river sediments.'' *Trans. Am. Geophysical Union*, 16, 463–467.
Toro-Escobar, C. M., Parker, G., and Paola, C. (1996). ''Transfer function for the deposition of poorly sorted gravel in response to streambed aggradation.'' *J. Hydr. Res.*, Delft, The Netherlands, 34(1), 35–54.
Vanoni, V. A., and Brooks, N. H. (1957). ''Laboratory studies of the roughness and suspended load of streams.'' *Rep. E68*, Sedimentation Lab., California Institute of Technology, Pasadena, Calif.
White, C. M. (1940). ''The equilibrium of grains on the bed of a stream.'' *Proc., Royal Soc.*, London, 174A.
Wiberg, P. L., and Smith, J. D. (1985). ''A theoretical model for saltating grains in water.'' *J. Geophys. Res.*, 90(C4), 7341–7354.
Wiberg, P. L., and Smith, J. D. (1987). ''Calculations of critical shear stress for motion of uniform and heterogeneous sediments.'' *Water Resour. Res.*, 23(8), 1471–1480.

APPENDIX II. NOTATION

The following symbols are used in this paper:

B = channel width (L);
C = dimensionless upstream volume sediment concentration;
c_D, c_L = dimensionless drag and lift coefficients of particle, respectively;
D = grain size (mm) (L);
$D_{\text{coarse }m}$, $D_{\text{fine }m}$ = grain size of coarse and fine modes in bimodal mixture (mm) (L), respectively;
D_{depg} = geometric mean grain size of composite of deposit samples (mm) (L);
D_{fg} = geometric mean grain size of feed sediment (mm) (L);
D_{f90}, D_{f50}, D_{f10} = grain size of feed such that 90, 50, 10% of sample is finer (mm) (L), respectively;
D_g = geometric mean size of deposit (mm) (L);
D_{ug}, D_{mg}, D_{dg}, D_{fg} = geometric mean grain size of upstream, middle, downstream, and front deposits (mm) (L), respectively;
D_{90}, D_{50}, D_{10} = grain size of deposit such that 90, 50, 10% of sample is finer (mm) (L), respectively;
F = Froude number (dimensionless);
F_D, F_{Gn}, F_{Gt}, F_L, F_R = drag, normal gravitational, tangential gravitational, lift, and resistance forces acting on particle (ML T^{-2}), respectively;
F_u = dimensionless coefficient relating fluid velocity acting on particle to shear velocity;
g = gravitational acceleration (L T^{-2});
H = flow depth (L);
k_s, k_{sf} = roughness height and estimate of roughness height based on feed sediment (L), respectively;
$\hat{L}$, $\hat{L}_0$ = dimensionless deposit length and initial dimensionless deposit length, respectively;
L_d, L_{d0} = deposit length and initial deposit length (L), respectively;
n_k = dimensionless number relating roughness height to grain size;
Q_{fs} = mass feed rate of sediment (M T^{-1});
Q_w = water discharge (L^3 T^{-1});
q_{fs} = volume feed rate of sediment per unit width (L^2 T^{-1});
R = $\rho_s/\rho - 1$ (dimensionless);
R = Reynolds number (dimensionless);
R_H, R_S = dimensionless terms defined in Eq. (23);
R_k = Reynolds number based on shear velocity and roughness height (dimensionless);
r = D/D_g (dimensionless);
r_b = hydraulic radius of bed region (L);
S = bed slope (dimensionless);
t, t_r, t_0 = time, run time, and initial time (T), respectively;
$\hat{t}$, $\hat{t}_0$ = dimensionless time and dimensionless initial time, respectively;
U = sectionally averaged flow velocity (L T^{-1});
u_p = effective flow velocity acting on particle (L T^{-1});
u_*, u_{*b} = shear velocity and shear velocity of bed region (L T^{-1}), respectively;
V_g = dimensionless downstream coarsen rate defined in Eq. (9);
x = streamwise coordinate (L);
x^* = x/L_d, dimensionless streamwise coordinate;
x_u, x_m, x_d, x_f = streamwise coordinates of centroid of upstream, middle, downstream, and front samples (L), respectively;
x_u^*, x_m^*, x_d^*, x_f^* = dimensionless streamwise coordinates of centroid of upstream, middle, downstream, and front samples;
Δ_F = height of propagational front (L);
δ_{bv} = viscous length scale associated with bed region (L);
δ_H, δ_R = dimensionless exponents defined in Eqs. (24) and (26), respectively;
δ_v = viscous length scale (L);
θ = slope angle of bed (dimensionless);
θ_f, θ_{fg} = friction angle and friction angle of mean grain size (dimensionless), respectively;
θ_r = angle of repose (dimensionless);
λ = dimensionless scale ratio, here equal to 1/3;
λ_p = dimensionless bed porosity;
μ, μ_g = Coulomb coefficient of friction and Coulomb coefficient of friction associated with mean grain size (dimensionless), respectively;
ν = kinematic viscosity of water (L^2 T^{-1});
ρ_s, ρ = sediment and water density (M L^{-3}), respectively;
σ_g, σ_{depg}, σ_{fg} = geometric standard deviation of a deposit sample, composite of deposit, and feed sediment (dimensionless), respectively;
σ_ψ, $\sigma_{f\psi}$ = arithmetic standard deviation of deposit sample and feed sediment (dimensionless), respectively;
τ_b, τ_{bc}, τ_{bgc} = boundary shear stress, critical boundary shear stress for sediment size D, and critical boundary shear stress for size D_g (M L^{-1} T^{-2}), respectively;

τ_c^*, τ_{c0}^* = critical Shields stress for sediment motion and critical Shields stress on horizontal bed (dimensionless), respectively;

τ_{fg}^* = Shields stress associated with size D_{fg} (dimensionless);

ψ, ψ_m, ψ_{mdep} = size on psi scale of grain, mean psi of a deposit sample, and mean psi size of composite of deposit samples (dimensionless), respectively; and

ψ_{um}, ψ_{dm} = mean size on psi scale of upstream and downstream deposit samples (dimensionless), respectively.